Learning from failure: boosting cycling endurance of optical phase change materials

Cosmin-Constantin Popescu[1], Steven Vitale[2], Christopher Roberts[2], Paul Miller[2], Kiumars Aryana[3], Myungkoo Kang[4], Kathleen Richardson[4], Hyun Jung Kim[3], William Humphreys[3], Tian Gu[1], Juejun Hu[1]

[1]Department of Materials Science and Engineering, Massachusetts Institute of Technology
[2]Lincoln Laboratory, Massachusetts Institute of Technology
[3]NASA Langley Research Center
[4]College of Optics and Photonics, University of Central Florida

ABSTRACT

Chalcogenide phase change materials (PCMs) are a unique class of compounds whose switchable optical and electronic properties have fueled an explosion of emerging applications in microelectronics and microphotonics. Key to any application is the ability of PCMs to reliably switch between crystalline and amorphous states over a large number of cycles. While this issue has been extensively studied in the case of microelectronic memories, current PCM-based optical devices suffer from much inferior endurance. To understand the failure mechanisms limiting endurance of PCMs specifically in microphotonic devices, we have developed an on-chip resistive micro-heater platform and an automatic multi-modal characterization system to analyze cycling performance of optical PCMs. Reversible switching of large-area PCM devices over 50,000 cycles was demonstrated.

Keywords: Phase change materials, reconfigurable photonics, endurance, reliability, integrated photonics, metasurfaces

1. INTRODUCTION

Phase change materials (PCMs) generally refer to a group of chalcogenide compounds which exhibit distinctively different electrical and optical properties in their amorphous (a-) and crystalline (c-) states[1–4]. These materials can be reversibly switched between the two structures as well as intermediate states (corresponding to mixtures of the two material phases) via transient thermal pulses[5–7]. The different levels are derived from either progressive phase transition where the two phases are spatially separated by a moving boundary[8], or intermediate states of PCMs containing crystalline phases precipitated from an amorphous matrix across the entire PCM volume[9]. They are also known to be non-volatile, i.e. capable of maintaining the structure state for an extended period when the thermal stimuli are removed[10]. Furthermore, it has been shown that PCMs can offer giant index change without incurring optical absorption[11–14], a crucial advantage over free-carrier based modulation. These collections of remarkable attributes have motivated a surge of interest in their applications in reconfigurable photonics in recent years[15–26]. Examples of emerging PCM-based devices include photonic memories[27–30], reflective displays (similar to electronic papers)[31–35], self-holding optical switching devices[36–44] for signal routing (e.g. in data centers[45] or wavelength division multiplexing networks[46]), reconfigurable metasurface optics[47–54] exemplified by zoom or autofocus lenses[55,56], programmable photonic circuits[57–62], optical limiters[63], smart glazing[64], adaptive optics with giant tunability[65–67], and neuromorphic optical computing systems by mimicking the complex behavior of synapses and neural circuits[68–72].

*hujuejun@mit.edu; phone 1-302-766-3083

This material is based upon work supported by the Under Secretary of Defense for Research and Engineering under Air Force Contract No. FA8702-15-D-0001. Any opinions, findings, conclusions or recommendations expressed in this material are those of the author(s) and do not necessarily reflect the views of the Under Secretary of Defense for Research and Engineering.

Large switching endurance, i.e. long cycling lifetime, is a key requirement for most photonic applications. While PCM endurance has been heavily vetted for electrical data storage, the distinct switching mechanisms and material compositions employed in photonics entail unresolved challenges that limit current low-loss PCMs' endurance[73]. To understand the failure mechanisms limiting endurance of PCMs specifically in photonic devices, we have developed an on-chip micro-heater platform and an automatic multi-modal characterization system to analyze cycling performance of optical PCMs.

2. MICRO-HEATER PLATFORM

The fabrication process flow of the micro-heater platform is illustrated in Figure 1. The micro-heaters were fabricated on a silicon-on-insulator (SOI) platform with 220 nm Si on 3 µm SiO_2. The heater fabrication was carried out at the Lincoln Laboratories foundry. The n++ doped regions were implanted with phosphorous ions at 80 kV and 10^{16} cm^{-2} area doping density followed by rapid thermal annealing for 10 s at 1000 °C. The doping region can be seen in (Figure 1) with heater sizes from 100 to 200 µm. Another way to dope the silicon can be done via spin coating and patterning spin-on-dopant. 10 nm of SiO_2 were grown on the device and an etch to the doped Si regions was performed. An adhesion layer of 10 nm Ti and 20 nm TiN was deposited, followed by an etch back to define the contact regions with the doped Si. 350 nm of Al were deposited for contacts. The chip was patterned with photolithography using 2 µm AZ nLOF 2035, and developed with AZ 300 MIF. The PCM was deposited via thermal evaporation in a custom system from PVD Products Inc. at a typical base pressure of 2×10^{-6} Torr from a pre-weighted source to exhaustion. The mass was pre-calibrated for a target thickness. Depositions were done with total film thicknesses of 50 nm up to 180 nm. R.D. Mathis Tantalum baffle boats were used as source material carriers and resistive elements for heating. A pre-soak step of 4 minutes was done before increasing the power to the boat and initiating the deposition. The substrate was neither heated nor rotated during the deposition. The photoresist was removed in acetone. The GSST was encapsulated via atomic layer deposition in 20 nm Al_2O_3 and then further encapsulated in a thicker protective layer. This second layer was plasma enhanced CVD SiN_x. The deposited protective layer is removed from above the contact pads using SF_6 and Ar reactive ion etching (RIE) or CHF_3 and CF_4 RIE using a hard-baked AZ 3312 mask. After the etch-back, the remaining resist is removed via O_2 plasma ashing. The heaters are connected to a printed circuit board via wire bonding with gold wire using a ball bonder.

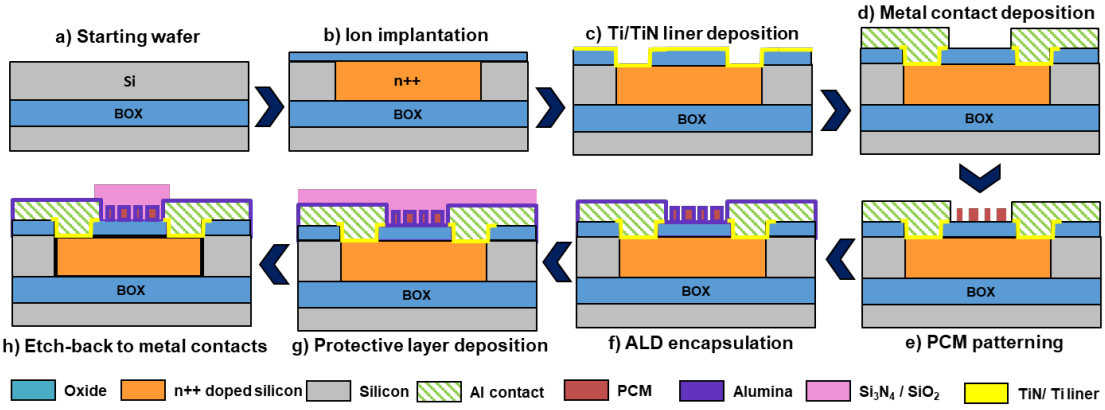

Figure 1. Schematic fabrication process flow of the micro-heater platform for PCM characterization

To trigger the phase transition in the PCM, the voltage source used was a Keithley 2200-60-2 connected via USB-A to USB-B. The function generator was an Agilent 33250 A with an RS-232 with null modem converter for serial data communication to USB. The null modem is needed for appropriate serial communication as the transmission and reception lines are switched in the function generator. BNC connectors were used to connect the output of the function generator and voltage source to an N-channel MOSFET IRF 510 (power MOSFET for high power and voltage applications) used for controlling the voltage pulse width. The control of the pulse width is done by connecting the positive end of the function generator to the gate of the transistor, the device under test (DUT) (i.e. the heater) is connected in series with the drain of the transistor and then the positive end of the voltage supply is subsequently connected. Optionally, for better shape fidelity of the pulse (i.e. removing high frequency noise in the signal) bypass capacitors can be connected between the power supply and ground. The DUT should not be placed in series with the source of the transistor as this will introduce an RC behavior into the transistor and slow down the opening and closing process of the circuit. Ideally, the source is connected to common ground. A diagram of the schematic can be found in Figure 2. While further methods can be enabled to smooth the electric pulse, the system is slowed down by the thermal behavior of the heater and thus the shown schematic provides

adequate results. The DUT will normally sit at high voltage during the testing of the sample and the end of one of the heater pads will drop to ground, allowing current flow, only when the function generator provides a pulse to the gate of the MOSFET. The voltage given to the gate of the MOSFET can be found in the Drain-to-Source voltage diagram of the part but typically should be between 3 and 5 V to "turn on" the transistor. The sample is connected to this circuit via wire bonding using a printed circuit board (PCB) and various connectors can then be used to connect the PCB to the system, one method being the use of BNC to DuPont wire connectors.

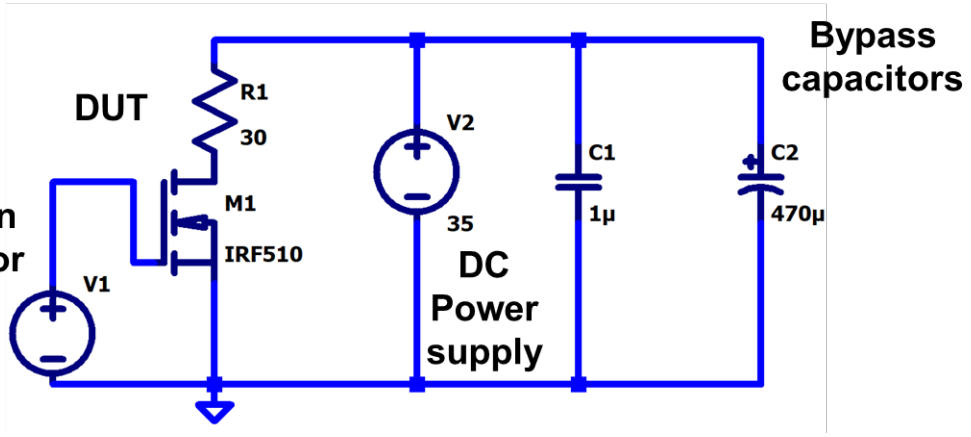

Figure 2. Electric diagram of the circuit for voltage pulse generation with values for pulses provided for controlling the MOSFET. V1 is the function generator and V2 is the voltage source.

A CMOS color Thorlabs DCC1645C-HQ camera has been used for optical imaging connected via USB to the control computer. A white correction should be done prior to beginning the measurements. Using a gray card in front of the microscope with the lamp at maximum intensity on the objective desired, automatic white balance and the gains of the three color channels can be established such that the mean values across the three color channels are equal. For verification, a histogram of the RGB values can be analyzed on the same gray card and the three mean values should be equal, ideally in the middle of the scale (124 for 0 to 255). This serves to remove artifacts in the reproduced color originating from the light source intensity distribution.

The SOI platform allows for tests in both transmission and reflection in the near IR along with cycling the device to highlight any potential issues during the lifetime of the PCM. It can be used to analyze optical and structural properties of patterned micron and sub-micron PCM structures, including their time-temperature-transformation (TTT) diagrams[7]. Because of the size of the doped silicon heaters, the platform further allows analysis and statistics of multiple PCM structures simultaneously, being able to highlight geometry dependent behavior. Moreover, it can be used to analyze structures that are several nanometers thin up to the micron level thick, values that span typical PCM films for waveguide integration up to dimensions for free space metasurfaces or spatial light modulators.

3. CHARACTERIZATION OF PCM CYCLING BEHAVIOR

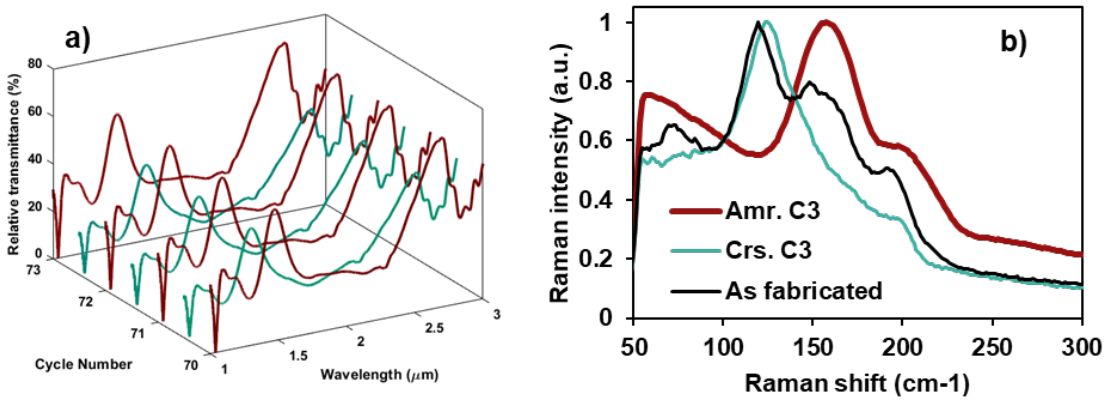

Figure 3. Examples of (a) infrared transmission and (b) Raman spectra of PCM switched with the micro-heater

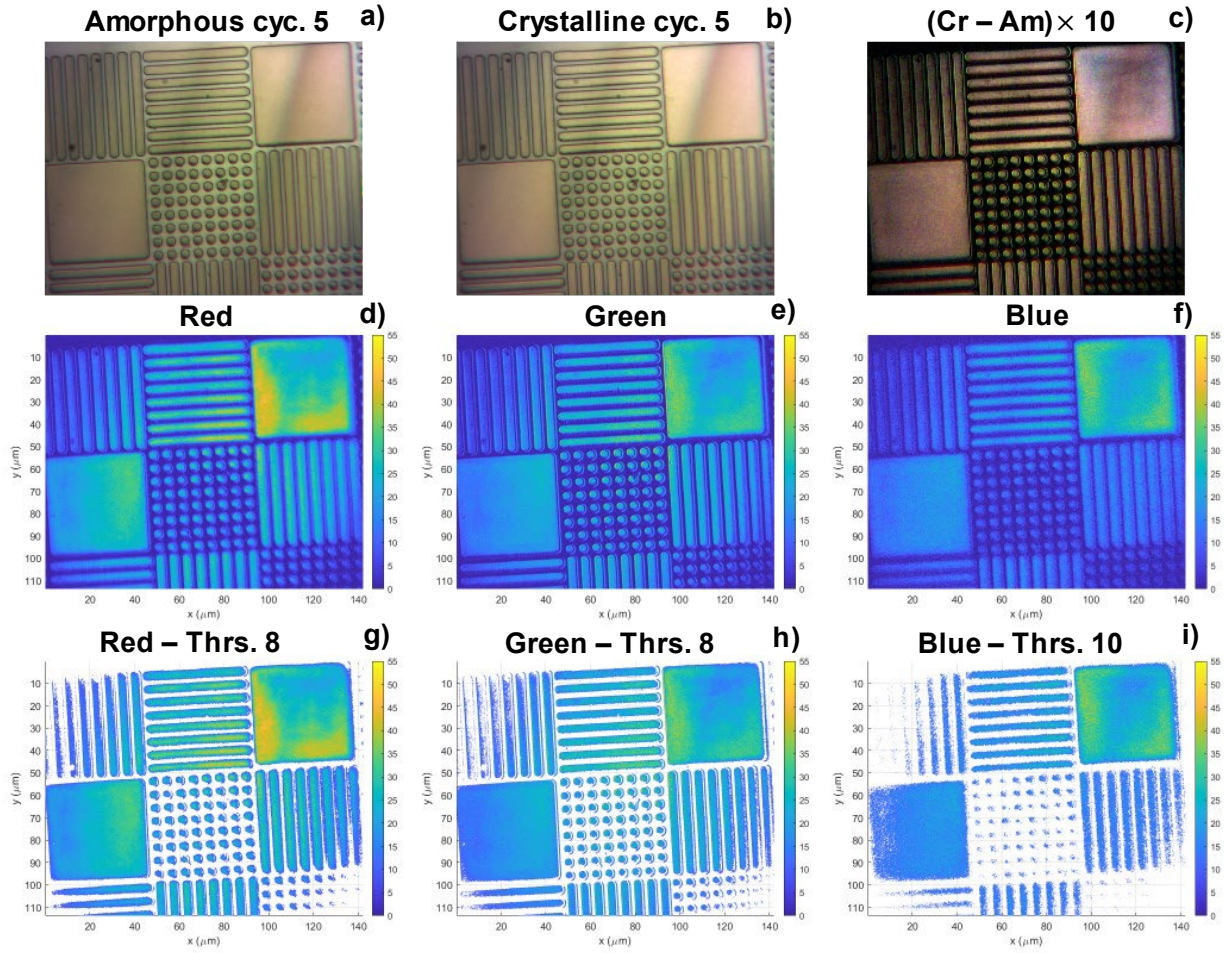

Figure 4. Visual illustration of the steps to compute the DMA mask - starting with the optical images in the amorphous a) and crystalline b) state for the device. The difference image between the two images multiplied by 10 for easier visualization c) followed by the difference image (no multiplication) across the three-color channels d-f) and the same images filtered by the threshold values shown above the image so that noise and the background/non-switching regions

are removed g-i). The color bars represent the value of the image on the 0 to 255 scale of the camera. The pitch of all the structures was 5 µm and the thin films were squares with sides of around 36 µm.

Figure 3 illustrates exemplary infrared transmission and Raman spectra of PCM (in this case $Ge_2Sb_2Se_4Te$, GSST) film switched with the micro-heater and measured *in situ* in between switching tests. The data indicate reliable reversible switching of the film between the amorphous and crystalline phases. To characterize the switching endurance, the optical contrast over switching cycles is recorded using the color camera and processed using differential mean analysis (DMA). In this method, the optical contrast between crystalline and amorphous states is calculated across the RGB channels and a threshold value is established for each channel to sort pixels in regions "with PCM" and regions "without PCM". A pixel is assigned as "with PCM" if the difference at the location between two states is above the threshold (Figure 4g-i). The assumption of the method is that if there is large enough contrast between the two images (or pixels for a specific position) then that will show as a large value in the difference matrix. Potentially, the absolute value of the difference matrix can be used instead, ignoring the assumption that typically the crystalline state will have higher reflectivity, but via manual inspection it can be seen that typically the assumption is followed and that the results should not be significantly different between using the absolute value of the difference or the signed value unless sample drift or illumination changes occur. Different thresholds may have to be selected between the three channels as different noise levels will be present and this method serves in part to remove the noise partially. Once the filtered regions are established across the three color channels, their overlap is taken as a large matrix / mask for where the PCM was switched. The mean RGB values of the pixels in the mask region is then obtained and divided by the mean RGB value of the pixels outside the mask. This is done to account for brightness changes in the image. Mathematically, this can be expressed as

$$\Delta DMA_{RGB} = \frac{\overline{\imath cr \in [\delta R \cup \delta G \cup \delta B]}}{\overline{\imath cr \notin [\delta R \cup \delta G \cup \delta B]}} - \frac{\overline{\imath am \in [\delta R \cup \delta G \cup \delta B]}}{\overline{\imath am \notin [\delta R \cup \delta G \cup \delta B]}}$$

where δ signifies the regions of the image where the image contrast between two states is above the set threshold. This value can be tracked over time and used, especially if quantification of what percentage of structures are still operational (i.e. provide optical contrast) is necessary. For DMA, this quantity is labeled viable pixels (for the pixels in the mask) and switching fraction. In principle, sample drift will show up in the viable pixel area but, in principle, it should not impact the Δ DMA values significantly because they are differences of means in regions where switching was detected, regardless if those are the same areas as in the previous images.

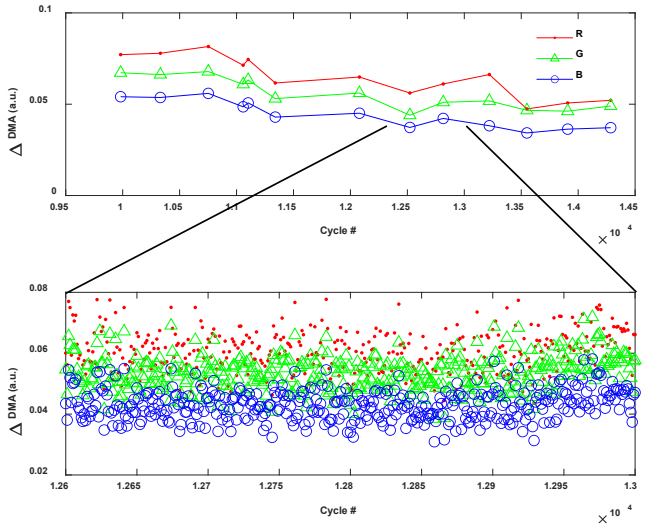

Figure 5. An example of measured ΔDMA on a PCM device over 10,000 switching cycles

The heater platform provides a facile method to examine cycling endurance of PCMs and we were able to iteratively improve the material and device processing to mitigate the failure mechanisms identified in these structures. Figure 5 shows an example of measured ΔDMA on a PCM device. The device exhibits stable switching response over more than 10,000 switching cycles. With improved PCM deposition protocols and encapsulation material processing, our latest PCM

devices have demonstrated endurance of over 57,000 cycles. We believe that the endurance performance can be further enhanced with optimized device designs.

4. SUMMARY

To fulfill the promises of PCMs, the stability of their phase change properties must be ensured during cycling. We have developed a micro-heater platform to support multi-modal characterization of PCMs during cyclic switching. We foresee that the wafer-scale PCM characterization platform described herein can be coupled with high-throughput computational methods[74–76] and combinatorial PCM synthetic approaches[77] to significantly expedite the discovery and validation of optical PCMs with enhanced endurance performance.

ACKNOWLEDGEMENTS

This material is based upon work supported by the Assistant Secretary of Defense for Research and Engineering under Air Force Contract No. FA8721-05-C-0002 and/or FA8702-15-D-0001, and by the NSF under award number 2132929. The views, opinions and/or findings expressed are those of the authors and should not be interpreted as representing the official views or policies of the Department of Defense or the U.S. Government.

REFERENCES

[1] Wuttig, M., Bhaskaran, H., and Taubner, T., "Phase-change materials for non-volatile photonic applications," Nature Photonics 11(8), 465–476 (2017).

[2] Zhang, W., Mazzarello, R., and Ma, E., "Phase-change materials in electronics and photonics," MRS Bulletin 44(09), 686–690 (2019).

[3] Elliott, S.R., "Chalcogenide Phase-Change Materials: Past and Future," International Journal of Applied Glass Science 6(1), 15–18 (2015).

[4] Zhang, Y., Ríos, C., Shalaginov, M.Y., Li, M., Majumdar, A., Gu, T., and Hu, J., "Myths and truths about optical phase change materials: A perspective," Applied Physics Letters 118(21), 210501 (2021).

[5] Li, X., Youngblood, N., Ríos, C., Cheng, Z., Wright, C.D., Pernice, W.H., and Bhaskaran, H., "Fast and reliable storage using a 5 bit, nonvolatile photonic memory cell," Optica 6(1), 1 (2019).

[6] Sevison, G.A., Farzinazar, S., Burrow, J.A., Perez, C., Kwon, H., Lee, J., Asheghi, M., Goodson, K.E., Sarangan, A., et al., "Phase Change Dynamics and Two-Dimensional 4-Bit Memory in Ge2Sb2Te5 via Telecom-Band Encoding," ACS Photonics 7(2), 480–487 (2020).

[7] Ríos, C., Zhang, Y., Shalaginov, M.Y., Deckoff-Jones, S., Wang, H., An, S., Zhang, H., Kang, M., Richardson, K.A., et al., "Multi-Level Electro-Thermal Switching of Optical Phase-Change Materials Using Graphene," Advanced Photonics Research 2(1), 2000034 (2020).

[8] Rios, C., Stegmaier, M., Cheng, Z., Youngblood, N., Wright, C.D., Pernice, W.H.P., and Bhaskaran, H., "Controlled switching of phase-change materials by evanescent-field coupling in integrated photonics [Invited]," Optical Materials Express 8(9), 2455 (2018).

[9] Zhang, Y., Fowler, C., Liang, J., Azhar, B., Shalaginov, M.Y., Deckoff-Jones, S., An, S., Chou, J.B., Roberts, C.M., et al., "Electrically reconfigurable non-volatile metasurface using low-loss optical phase-change material," Nature Nanotechnology 16, 661–666 (2021).

[10] Youngblood, N., Ríos, C., Gemo, E., Feldmann, J., Cheng, Z., Baldycheva, A., Pernice, W.H., David Wright, C., Bhaskaran, H., et al., "Tunable Volatility of Ge2Sb2Te5 in Integrated Photonics," Advanced Functional Materials 29(11), 1807571 (2019).

[11] Zhang, Y., Li, J., Chou, J., Fang, Z., Yadav, A., Lin, H., Du, Q., Michon, J., Han, Z., et al., "Broadband Transparent Optical Phase Change Materials," in Conference on Lasers and Electro-Optics, JTh5C.4 (2017).

[12] Zhang, Y., Chou, J.B., Li, J., Li, H., Du, Q., Yadav, A., Zhou, S., Shalaginov, M.Y., Fang, Z., et al., "Broadband transparent optical phase change materials for high-performance nonvolatile photonics," Nature Communications 10, 4279 (2019).

[13] Delaney, M., Zeimpekis, I., Lawson, D., Hewak, D.W., and Muskens, O.L., "A New Family of Ultralow Loss Reversible Phase-Change Materials for Photonic Integrated Circuits: Sb2S3 and Sb2Se3," Advanced Functional Materials 30(36), 2002447 (2020).

[14] Dong, W., Liu, H., Behera, J.K., Lu, L., Ng, R.J.H., Sreekanth, K.V., Zhou, X., Yang, J.K.W., and Simpson, R.E., "Wide Bandgap Phase Change Material Tuned Visible Photonics," Advanced Functional Materials 29(6), 1806181 (2019).
[15] Wang, J., Wang, L., and Liu, J., "Overview of Phase-Change Materials Based Photonic Devices," IEEE Access 8, 121211–121245 (2020).
[16] Wang, X., Qi, H., Hu, X., Yu, Z., Ding, S., Du, Z., and Gong, Q., "Advances in Photonic Devices Based on Optical Phase-Change Materials," Molecules 26(9), 2813 (2021).
[17] Nisar, M.S., Yang, X., Lu, L., Chen, J., and Zhou, L., "On-Chip Integrated Photonic Devices Based on Phase Change Materials," Photonics 8(6), 205 (2021).
[18] Cao, T., and Cen, M., "Fundamentals and Applications of Chalcogenide Phase-Change Material Photonics," Advanced Theory and Simulations 2(8), 1900094 (2019).
[19] Wright, C.D., Bhaskaran, H., and Pernice, W.H.P., "Integrated phase-change photonic devices and systems," MRS Bulletin 44(9), 721–727 (2019).
[20] Zhou, W., Farmakidis, N., Feldmann, J., Li, X., Tan, J., He, Y., Wright, C.D., Pernice, W.H.P., and Bhaskaran, H., "Phase-change materials for energy-efficient photonic memory and computing," MRS Bulletin 47(5), 502–510 (2022).
[21] Fang, Z., Chen, R., Zheng, J., and Majumdar, A., "Non-Volatile Reconfigurable Silicon Photonics Based on Phase-Change Materials," IEEE Journal of Selected Topics in Quantum Electronics 28(3), 8200317 (2022).
[22] Abdollahramezani, S., Hemmatyar, O., Taghinejad, H., Krasnok, A., Kiarashinejad, Y., Zandehshahvar, M., Alù, A., and Adibi, A., "Tunable nanophotonics enabled by chalcogenide phase-change materials," Nanophotonics 9, 1189–1241 (2020).
[23] Brückerhoff-Plückelmann, F., Feldmann, J., Wright, C.D., Bhaskaran, H., and Pernice, W.H.P., "Chalcogenide phase-change devices for neuromorphic photonic computing," Journal of Applied Physics 129(15), 151103 (2021).
[24] Simpson, R.E., Yang, J.K.W., Yang, J.K.W., and Hu, J., "Are phase change materials ideal for programmable photonics?: opinion," Optical Materials Express 12(6), 2368–2373 (2022).
[25] Zheng, C., Simpson, R.E., Tang, K., Ke, Y., Nemati, A., Zhang, Q., Hu, G., Lee, C., Teng, J., et al., "Enabling Active Nanotechnologies by Phase Transition: From Electronics, Photonics to Thermotics," Chemical Reviews (2022).
[26] Guo, P., Sarangan, A.M., and Agha, I., "A review of germanium-antimony-telluride phase change materials for non-volatile memories and optical modulators," Applied Sciences 9(3), 530 (2019).
[27] Rios, C., Stegmaier, M., Hosseini, P., Wang, D., Scherer, T., Wright, C.D., Bhaskaran, H., and Pernice, W.H.P., "Integrated all-photonic non-volatile multi-level memory," Nature Photonics 9(11), 725–732 (2015).
[28] Rios, C., Hosseini, P., Wright, C.D., Bhaskaran, H., and Pernice, W.H.P., "On-chip photonic memory elements employing phase-change materials," Advanced Materials 26, 1372–1377 (2014).
[29] Cheng, Z., Ríos, C., Youngblood, N., Wright, C.D., Pernice, W.H.P., and Bhaskaran, H., "Device-Level Photonic Memories and Logic Applications Using Phase-Change Materials," Advanced Materials 30(32), 1802435 (2018).
[30] Meng, J., Peserico, N., Ma, X., Zhang, Y., Popescu, C.-C., Kang, M., Miscuglio, M., Richardson, K., Hu, J., et al., "Electrical Programmable Low-loss high cyclable Nonvolatile Photonic Random-Access Memory," arXiv:2203.13337 (2022).
[31] Hosseini, P., Wright, C.D., and Bhaskaran, H., "An optoelectronic framework enabled by low-dimensional phase-change films," Nature 511(7508), 206–211 (2014).
[32] Ji, H.K., Tong, H., Qian, H., Hui, Y.J., Liu, N., Yan, P., and Miao, X.S., "Non-binary Colour Modulation for Display Device Based on Phase Change Materials," Scientific Reports 6, 39206 (2016).
[33] Ni, Z., Mou, S., Zhou, T., and Cheng, Z., "Broader color gamut of color-modulating optical coating display based on indium tin oxide and phase change materials," Applied Optics 57, 3385–3389 (2018).
[34] Wang, J., Li, Q., Tao, S., Xia, Z., Li, Y., Liu, Y., Gu, Z., and Hu, C., "Improving the reflectance and color contrasts of phase-change materials by vacancy reduction for optical-storage and display applications," Optics Letters 45(1), 244 (2020).
[35] Ríos, C., Hosseini, P., Taylor, R.A., and Bhaskaran, H., "Color Depth Modulation and Resolution in Phase-Change Material Nanodisplays," Advanced Materials 28(23), 4720–4726 (2016).
[36] Zhang, Q., Zhang, Y., Li, J., Soref, R., Gu, T., and Hu, J., "Broadband nonvolatile photonic switching based on optical phase change materials: beyond the classical figure-of-merit," Optics Letters 43(1), 94–97 (2018).

[37] Wang, N., Zhang, H., Zhou, L., Lu, L., Chen, J., and Rahman, B.M.A., "Design of Ultra-Compact Optical Memristive Switches with GST as the Active Material," Micromachines 10(7), 453 (2019).
[38] Ali, N., and Kumar, R., "Mid-infrared non-volatile silicon photonic switches using nanoscale Ge2Sb2Te5 embedded in silicon-on-insulator waveguides," Nanotechnology 31(11), 115207 (2020).
[39] Dhingra, N., Song, J., Saxena, G.J., Sharma, E.K., and Rahman, B.M.A., "Design of a Compact Low-Loss Phase Shifter Based on Optical Phase Change Material," IEEE Photonics Technology Letters 31(21), 1757–1760 (2019).
[40] Zhang, B., Li, Y., Fu, Q., Dai, T., Yu, H., Yang, J., Chen, W., Wang, P., Dai, S., et al., "Switchable Polarization Beam Splitter Based on GST-on-Silicon Waveguides," IEEE Photonics Journal 12(2), (2020).
[41] Xu, P., Zheng, J., Doylend, J.K., and Majumdar, A., "Low-Loss and Broadband Nonvolatile Phase-Change Directional Coupler Switches," ACS Photonics 6(2), 553–557 (2019).
[42] Zheng, J., Fang, Z., Wu, C., Zhu, S., Xu, P., Doylend, J.K., Deshmukh, S., Pop, E., Dunham, S., et al., "Nonvolatile Electrically Reconfigurable Integrated Photonic Switch Enabled by a Silicon PIN Diode Heater," Advanced Materials 32(31), 2001218 (2020).
[43] Fang, Z., Chen, R., Zheng, J., Khan, A.I., Neilson, K.M., Geiger, S.J., Callahan, D.M., Moebius, M.G., Saxena, A., et al., "Ultra-low-energy programmable non-volatile silicon photonics based on phase-change materials with graphene heaters," Nature Nanotechnology 17(8), 842–848 (2022).
[44] Ríos, C., Du, Q., Zhang, Y., Popescu, C.-C., Shalaginov, M.Y., Miller, P., Roberts, C., Kang, M., Richardson, K.A., et al., "Ultra-compact nonvolatile photonics based on electrically reprogrammable transparent phase change materials," PhotoniX 3, 26 (2022).
[45] Cheng, Q., Rumley, S., Bahadori, M., and Bergman, K., "Photonic switching in high performance datacenters [Invited]," Optics Express 26(12), 16022 (2018).
[46] Strasser, T.A., and Wagener, J.L., "Wavelength-selective switches for ROADM applications," IEEE Journal on Selected Topics in Quantum Electronics 16(5), 1150–1157 (2010).
[47] Shalaginov, M.Y., An, S., Zhang, Y., Yang, F., Su, P., Liberman, V., Chou, J.B., Roberts, C.M., Kang, M., et al., "Reconfigurable all-dielectric metalens with diffraction-limited performance," Nature Communications 12, 1225 (2021).
[48] An, S., Fowler, C., Zheng, B., Shalaginov, M.Y., Tang, H., Li, H., Zhou, L., Ding, J., Agarwal, A.M., et al., "A Deep Learning Approach for Objective-Driven All-Dielectric Metasurface Design," ACS Photonics 6(12), 3196–3207 (2019).
[49] Ee, H.S., and Agarwal, R., "Electrically programmable multi-purpose nonvolatile metasurface based on phase change materials," Physica Scripta 94(2), 025803 (2019).
[50] An, S., Zheng, B., Tang, H., Shalaginov, M.Y., Zhou, L., Li, H., Kang, M., Richardson, K.A., Gu, T., et al., "Multifunctional Metasurface Design with a Generative Adversarial Network," Advanced Optical Materials 9, 2001433 (2021).
[51] An, S., Zheng, B., Julian, M., Williams, C., Tang, H., Gu, T., Zhang, H., Kim, H.J., and Hu, J., "Deep neural network enabled active metasurface embedded design," Nanophotonics 11(17), 4149–4158 (2022).
[52] Nemati, A., Wang, Q., Hong, M., and Teng, J., "Tunable and reconfigurable metasurfaces and metadevices," Opto-Electronic Advances 1(5), 18000901–18000925 (2018).
[53] Wang, Q., Rogers, E.T.F.T.F., Gholipour, B., Wang, C.-M., Yuan, G., Teng, J., and Zheludev, N.I.I., "Optically reconfigurable metasurfaces and photonic devices based on phase change materials," Nature Photonics 10(1), 60–65 (2016).
[54] Gu, T., Kim, H.J., Rivero-Baleine, C., and Hu, J., "Reconfigurable metasurfaces towards commercial success," Nature Photonics 17(1), 48–58 (2023).
[55] Yang, F., Lin, H.-I., Shalaginov, M.Y., Stoll, K., An, S., Rivero-Baleine, C., Kang, M., Agarwal, A., Richardson, K., et al., "Reconfigurable parfocal zoom metalens," Advanced Optical Materials 10, 2200721 (2022).
[56] Yin, X., Steinle, T., Huang, L., Taubner, T., Wuttig, M., Zentgraf, T., and Giessen, H., "Beam switching and bifocal zoom lensing using active plasmonic metasurfaces," Light: Science & Applications 6(7), e17016 (2017).
[57] Bogaerts, W., Pérez, D., Capmany, J., Miller, D.A.B., Poon, J., Englund, D., Morichetti, F., and Melloni, A., "Programmable photonic circuits," Nature 586, 207–216 (2020).
[58] Pérez, D., Gasulla, I., Crudgington, L., Thomson, D.J., Khokhar, A.Z., Li, K., Cao, W., Mashanovich, G.Z., and Capmany, J., "Multipurpose silicon photonics signal processor core," Nature Communications 8, 636 (2017).
[59] Shen, Y., Harris, N.C., Skirlo, S., Prabhu, M., Baehr-Jones, T., Hochberg, M., Sun, X., Zhao, S., Larochelle, H., et al., "Deep learning with coherent nanophotonic circuits," Nature Photonics 11(7), 441–446 (2017).

[60] Kita, D.M., Miranda, B., Favela, D., Bono, D., Michon, J., Lin, H., Gu, T., and Hu, J., "High-performance and scalable on-chip digital Fourier transform spectroscopy," Nature Communications 9(1), 4405 (2018).
[61] Liao, K., Chen, Y., Yu, Z., Hu, X., Wang, X., Lu, C., Lin, H., Du, Q., Hu, J., et al., "All-optical computing based on convolutional neural networks," Opto-Electronic Advances 4(11), 200060- (2021).
[62] Liao, K., Li, C., Dai, T., Zhong, C., Lin, H., Hu, X., and Gong, Q., "Matrix eigenvalue solver based on reconfigurable photonic neural network," Nanophotonics (2022).
[63] Sarangan, A., Duran, J., Vasilyev, V., Limberopoulos, N., Vitebskiy, I., and Anisimov, I., "Broadband Reflective Optical Limiter Using GST Phase Change Material," IEEE Photonics Journal 10(2), 2200409 (2018).
[64] Youngblood, N., Talagrand, C., Porter, B.F., Galante, C.G., Kneepkens, S., Triggs, G., Ghazi Sarwat, S., Yarmolich, D., Bonilla, R.S., et al., "Reconfigurable Low-Emissivity Optical Coating Using Ultrathin Phase Change Materials," ACS Photonics 9(1), 90–100 (2022).
[65] Chaudhary, K., Tamagnone, M., Yin, X., Spägele, C.M., Oscurato, S.L., Li, J., Persch, C., Li, R., Rubin, N.A., et al., "Polariton nanophotonics using phase-change materials," Nature Communications 10, 4487 (2019).
[66] Gholipour, B., Karvounis, A., Yin, J., Soci, C., MacDonald, K.F., and Zheludev, N.I., "Phase-change-driven dielectric-plasmonic transitions in chalcogenide metasurfaces," NPG Asia Materials 10(6), 533–539 (2018).
[67] Cueff, S., Taute, A., Bourgade, A., Lumeau, J., Monfray, S., Song, Q., Genevet, P., Devif, B., Letartre, X., et al., "Reconfigurable Flat Optics with Programmable Reflection Amplitude Using Lithography-Free Phase-Change Material Ultra-Thin Films," Advanced Optical Materials 9(2), 2001291 (2021).
[68] Feldmann, J., Youngblood, N., Wright, C.D., Bhaskaran, H., and Pernice, W.H.P., "All-optical spiking neurosynaptic networks with self-learning capabilities," Nature 569, 208–214 (2019).
[69] Xu, M., Mai, X., Lin, J., Zhang, W., Li, Y., He, Y., Tong, H., Hou, X., Zhou, P., et al., "Recent Advances on Neuromorphic Devices Based on Chalcogenide Phase-Change Materials," Advanced Functional Materials 30(50), 2003419 (2020).
[70] Zhuge, X., Wang, J., and Zhuge, F., "Photonic Synapses for Ultrahigh-Speed Neuromorphic Computing," physica status solidi (RRL) – Rapid Research Letters 13(9), 1900082 (2019).
[71] Cheng, Z., Ríos, C., Pernice, W.H.P., David Wright, C., and Bhaskaran, H., "On-chip photonic synapse," Science Advances 3(9), e1700160 (2017).
[72] Chakraborty, I., Saha, G., Sengupta, A., and Roy, K., "Toward Fast Neural Computing using All-Photonic Phase Change Spiking Neurons," Scientific Reports 8, 12980 (2018).
[73] Martin-Monier, L., Popescu, C.-C., Ranno, L., Mills, B., Geiger, S., Callahan, D., Moebius, M., and Hu, J., "Endurance of Chalcogenide Optical Phase Change Materials: a Review," Optical Materials Express 12(6), 2145–2167 (2022).
[74] Hu, S., Liu, B., Li, Z., Zhou, J., and Sun, Z., "Identifying optimal dopants for Sb2Te3 phase-change material by high-throughput ab initio calculations with experiments," Computational Materials Science 165, 51–58 (2019).
[75] Pike, N.A., Matt, A., and Løvvik, O.M., "Determining the optimal phase-change material via high-throughput calculations," MRS Advances 4(50), 2679–2687 (2019).
[76] Kusne, A.G., Yu, H., Wu, C., Zhang, H., Hattrick-Simpers, J., DeCost, B., Sarker, S., Oses, C., Toher, C., et al., "On-the-fly closed-loop materials discovery via Bayesian active learning," Nature Communications 11, 5966 (2020).
[77] Guerin, S., Hayden, B., Hewak, D.W., and Vian, C., "Synthesis and Screening of Phase Change Chalcogenide Thin Film Materials for Data Storage," ACS Combinatorial Science 19(7), 478–491 (2017).